12-2017

Synthesis of magnetic carbon supported manganese catalysts for phenol oxidation by activation of peroxymonosulfate

Yuxian Wang

Yongbing Xie

Chunmao Chen

Xiaoguang Duan

Hongqi Sun
Edith Cowan University

See next page for additional authors

10.3390/catal7010003

Wang, Y., Xie, Y., Chen, C., Duan, X., Sun, H., & Wang, S. (2017). Synthesis of Magnetic Carbon Supported Manganese Catalysts for Phenol Oxidation by Activation of Peroxymonosulfate. *Catalysts*, *7*(1), 3. Available here

catalysts

MDPI

Article

Synthesis of Magnetic Carbon Supported Manganese Catalysts for Phenol Oxidation by Activation of Peroxymonosulfate

Yuxian Wang [1,*], Yongbing Xie [2], Chunmao Chen [1], Xiaoguang Duan [3], Hongqi Sun [4] and Shaobin Wang [3]

1 State Key Laboratory of Heavy Oil Processing, China University of Petroleum, Beijing, 18 Fuxue Road, Beijing 102249, China; chunmaochan@163.com
2 Beijing Engineering Research Center of Process Pollution Control, Key Laboratory of Green Process and Engineering, Institute of Process Engineering, Chinese Academy of Sciences, Beijing 100190, China; ybxie@ipe.ac.cn
3 Department of Chemical Engineering, Curtin University, GPO Box U1987, Perth 6845, Australia; xiaoguang.duan@postgrad.curtin.edu.au (X.D.); s.wang@curtin.edu.au (S.W.)
4 School of Engineering, Edith Cowan University, 270 Joondalup Drive, Joondalup 6027, Australia; h.sun@curtin.edu.au
* Correspondence: yuxian.wang@cup.edu.cn; Tel.: +86-10-8973-9078

Academic Editor: Keith Hohn
Received: 2 November 2016; Accepted: 21 December 2016; Published: 26 December 2016

Abstract: Magnetic core/shell nanospheres (MCS) were synthesized by a novel and facile one-step hydrothermal method. Supported manganese oxide nanoparticles (Fe_3O_4/C/Mn) were obtained from various methods (including redox, hydrothermal and impregnation) using MCS as the support material and potassium permanganate as the precursor of manganese oxide. The Mn/MCS catalysts were characterized by a variety of characterization techniques and the catalytic performances of Fe_3O_4/C/Mn nanoparticles were tested in activation of peroxymonosulfate to produce reactive radicals for phenol degradation in aqueous solutions. It was found that Fe_3O_4/C/Mn catalysts can be well dispersed and easily separated from the aqueous solutions by an external magnetic field. Kinetic analysis showed that phenol degradation on Fe_3O_4/C/Mn catalysts follows the first order kinetics. The peroxymonosulfate activation mechanism by Fe_3O_4/C/Mn catalysts for phenol degradation was then discussed.

Keywords: magnetic separation; sulfate radicals; Phenol; manganese oxides; carbon spheres

1. Introduction

Toxic and hazardous organic compounds, such as dyes and phenolic products, broadly exist in the wastewater generated from industrial processes and have caused severe problems to the environment [1,2]. Due to their strong toxicity even at low concentration [3], development of efficient treatment technologies is in urgent demand. Advanced oxidation processes (AOPs) involving Fenton reaction, photocatalysis, electrocatalysis and various chemical methods have attracted intensive research interests for decomposing the organic contaminants due to their high efficiency and complete degradation capability [4]. Previous investigations have demonstrated that Fenton/Fenton-like reactions utilizing hydroxyl radicals (OH·) could decompose organic contaminants efficiently [5,6]. However, these processes suffer from shortcomings like metal leaching, pH adjustment, production of large quantity of sludge and cost-intensive production [7].

As alternatives to hydroxyl radicals involved in Fenton reactions, sulfate radicals (SO_4^{-}) which can be generated by activation of peroxymonosulfate (Oxone, peroxymonosulfate (PMS)) have gain

intensive attention [8–10]. Sulfate radicals have a higher redox potential than hydroxyl radicals (E_0 = 3.1 V vs. E_0 = 2.7 V) and enable them to be more desirable for persistent organic pollutants (POPs) degradation [11]. Cobalt oxides are proven to be the effective heterogeneous catalysts for PMS activation [12,13]. Nevertheless, due to the metal leaching, employment of cobalt based catalysts would result in the secondary pollution caused by the toxicity of cobalt ions [14,15]. Moreover, improper recycling of these nanosized particles would also bring contaminant to the environment.

Utilizing magnetic separation for catalysts recycle has attracted considerable research attention. Compared with traditional separation technologies such as centrifugation and filtration, magnetic separation through an external magnetic field is more convenient and less cost-intensive [16]. Magnetite (Fe_3O_4) nanoparticles are prevalently employed as magnetic cores owing to their outstanding magnetic and electrochemical properties [17–20]. However, their high surface area to volume ratio and strong dipole–dipole attraction make them prone to aggregation, and the limited functional groups circumvent their further applications [16]. To circumvent such drawbacks, barrier materials have been investigated to prevent self-aggregation and to isolate from attached functional components [16,21]. Recently, carbon coated magnetite nanospheres (Fe_3O_4/C) have been employed because of their low cytotoxicity and highly modifiable surface [22,23]. In the pioneer study, we synthesized such magnetic carbon nanospheres and loaded with cobalt oxides as catalysts [24]. It was found that the as-synthesized materials demonstrated excellent recyclability under external magnetic field.

Compared to cobalt oxides, manganese oxides are less toxic and more abundant in earth. Due to the unique redox loop (Mn^{3+}/Mn^{4+} or Mn^{2+}/Mn^{3+}) involving a single electron transfer and the superior chemical and physical properties, manganese oxides demonstrate great potentials as catalysts [14]. In our previous studies, manganese oxides at different chemical states showed excellent catalytic abilities for PMS activation [13]. Although fruitful researches have been so far conducted for utilizing various manganese based catalysts for activation of PMS for environmental remediation, few studies focused on the supported manganese oxides catalysis [25].

In this study, three types of supported manganese oxide catalysts were prepared from redox, impregnation and hydrothermal methods, respectively, and magnetic carbon nanospheres (Fe_3O_4/C) were utilized as the supporting media. To evaluate morphological and physicochemical properties, the as-prepared catalysts were characterized by scanning electron microscopy (SEM), transmission electron microscopy (TEM), X-ray diffraction (XRD), N_2 sorption, Fourier Transform infrared spectroscopy (FT-IR) and thermogravimetric analysis (TGA) techniques. The heterogeneous catalytic performance of these catalysts was investigated by activation of PMS for oxidation of phenol solution and the reaction kinetics were investigated. Moreover, to better evaluate the catalytic performance of the as-prepared materials and the influence of electron donating group (EDG) and electron withdrawing group (EWG) on the degradation efficiency, p-cresol which including a methyl group (EDG) and 4-nitrophenol which including a nitro group (EWG) were utilized as the target pollutants.

2. Results and Discussion

2.1. Characterization of Fe_3O_4/C/Mn Hybrids

Figure 1 shows SEM images for investigation of the structure and the morphology of the samples. It can be found that all of the samples present a sphere-like morphology with a size range between 20 and 30 nm. Moreover, in these SEM images, the nanoparticles agglomerated to form bulk structures, which indicates the strong inter-molecular magnetic dipolar interaction induced by the magnetic core [22]. The Mn species were expected to homogeneously distribute on the spheres. Compared with Mn/MCS-H (Figure 1E), the morphology of Mn/MCS-R and Mn/MCS-I (Figure 1A,C) showed a more uniformed sphere-like structure, suggesting the calcination process in the two methods regulated the shape of hybrids.

Figure 2 displays TEM images of the as-synthesized magnetic carbon supported manganese catalysts. As seen, metal/carbon clusters were formed for all of these three samples. Fe_3O_4 (small bright dots) with a diameter of 10 nm and the amorphous carbon formed were found in the form of highly aggregated composites. For Mn/MCS-R, Mn/MCS-I, the large dart dots might refer to the formed manganese oxide. For Mn/MCS-H, beads/tubes structure was observed ascribing to the hydrothermal process.

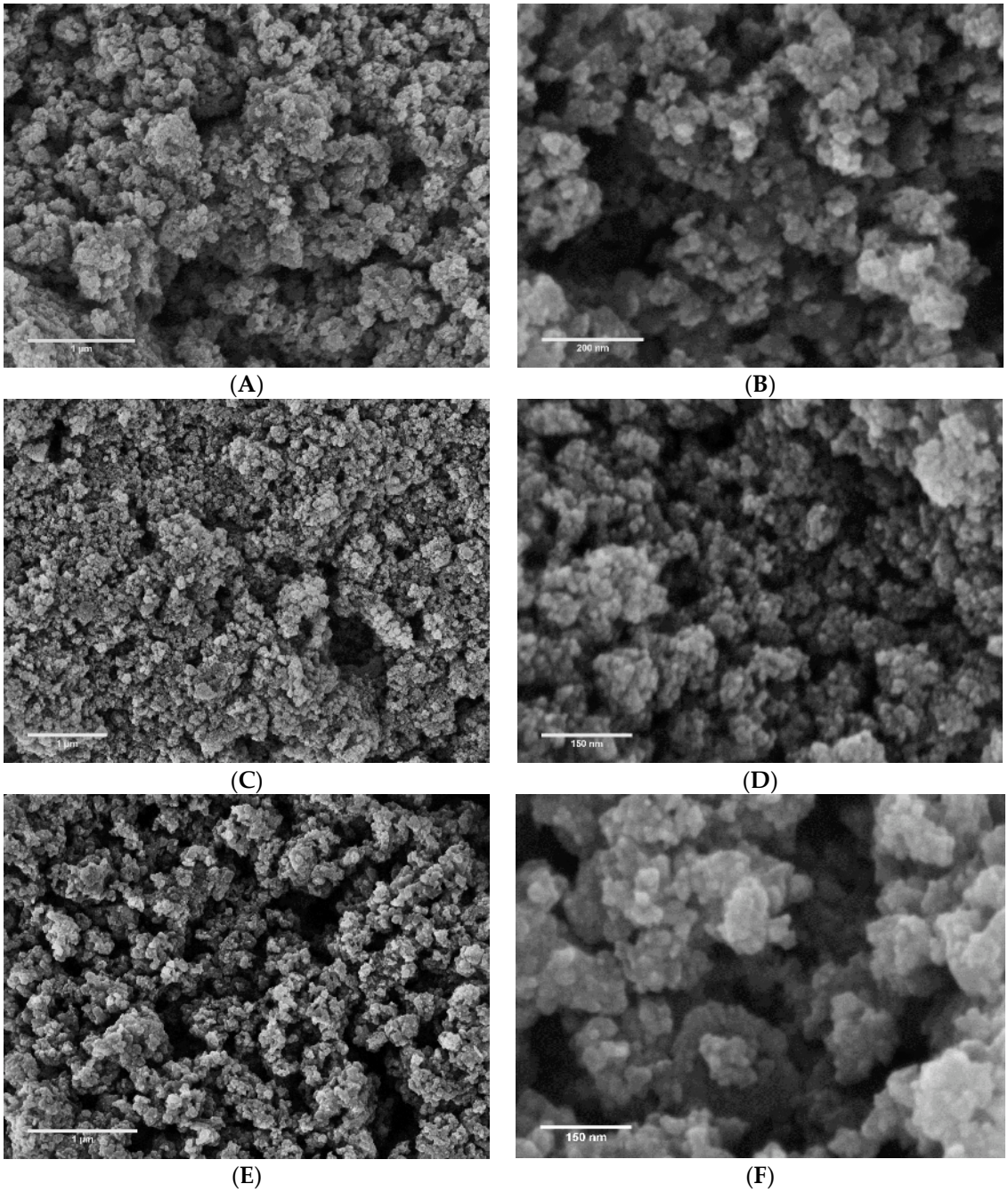

Figure 1. Scanning electron microscopy (SEM) images of Fe_3O_4/C/Mn hybrids: (**A**,**B**) from Fe_3O_4/C/Mn hybrid by redox method (Mn/MCS-R); (**C**,**D**) from Fe_3O_4/C/Mn hybrid by impregnation method (Mn/MCS-I); and (**E**,**F**) from Fe_3O_4/C/Mn hybrid by hydrothermal method (Mn/MCS-H).

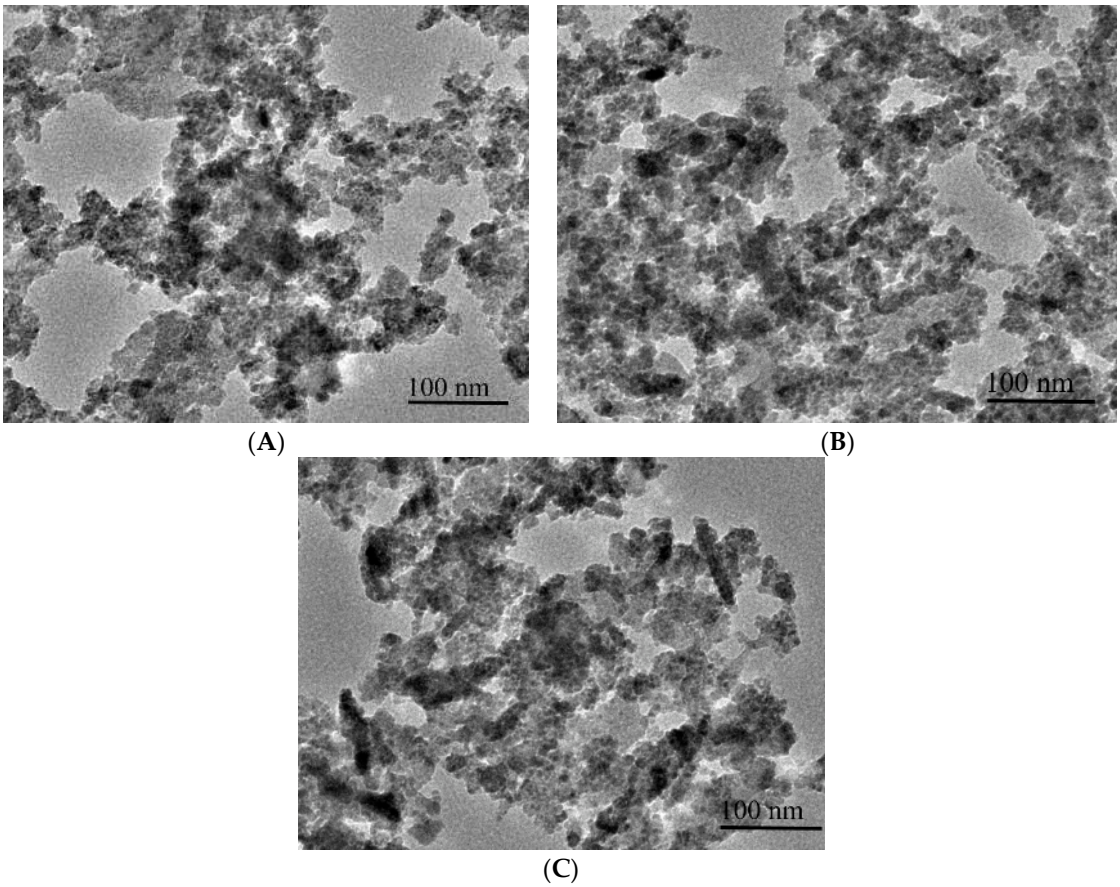

Figure 2. Transmission electron microscopy (TEM) images of: Mn/MCS-R (**A**); Mn/MCS-I (**B**); and Mn/MCS-H (**C**).

The crystalline structures of the samples were identified by XRD patterns, as shown in Figure 3. As seen, XRD patterns of the three magnetic carbon spheres (MCS) related samples had the same characteristic diffraction peaks at 30.1°, 35.4°, 43.1°, 56.9° and 62.5° and were well agreement with inverse spinal structure Fe_3O_4 with lattice constants of $\alpha = 8.397$ Å (JCPDS No. 65-3107) [26]. As illustrated in the figure, the characteristic peaks corresponded to crystal planes of (2 2 0), (3 1 1), (4 0 0), (4 2 2) and (4 4 0) of Fe_3O_4, respectively. Moreover, in all of these XRD patterns, no obvious sharp diffraction peaks (27° and 55°) corresponding to the graphite or graphite oxide can be observed [14], indicating that most of the carbon prepared with these methods was amorphous. For XRD patterns of Mn/MCS-R and Mn/MCS-I, no characteristic peaks were identified for MnO_x due to the heavy interference of Fe_3O_4 peaks and low manganese loading rate. However, for Mn/MCS-H, characteristic diffraction peaks for α-MnO_2 phase (JCPDS No. 44-0141, tetragonal, I4/m, $a = b = 9.78$ Å, $c = 2.86$ Å) were observed [27].

Figure 4 shows N_2 sorption isotherms and the pore size distributions of three Fe_3O_4/C/Mn hybrids. As seen, all the three samples presented a type IV isotherm with a type H3 hysteresis loop, indicating a typical mesoporous structure [24]. The hysteresis loops and pore size distributions (inset figure) for all of the samples are also quite similar: narrow hysteresis loops at a relative pressure P/P_0 range of 0.5 to 0.95 could be observed with single modal pore diameter distribution centered at around 2.5 nm. The BET surface area and the pore volume for each sample are summarized in Table 1. Mn/MCS-I showed the highest specific surface area which is almost three times higher than that of Mn/MCS-H (74.6 vs. 26.6 m^2/g). Correspondingly, the pore volumes follow the order of Mn/MCS-I > Mn/MCS-R > Mn/MCS-H. The high surface area and pore volume of sample Mn/MCS-I might be ascribed to the calcination involved in the sample synthesis processes.

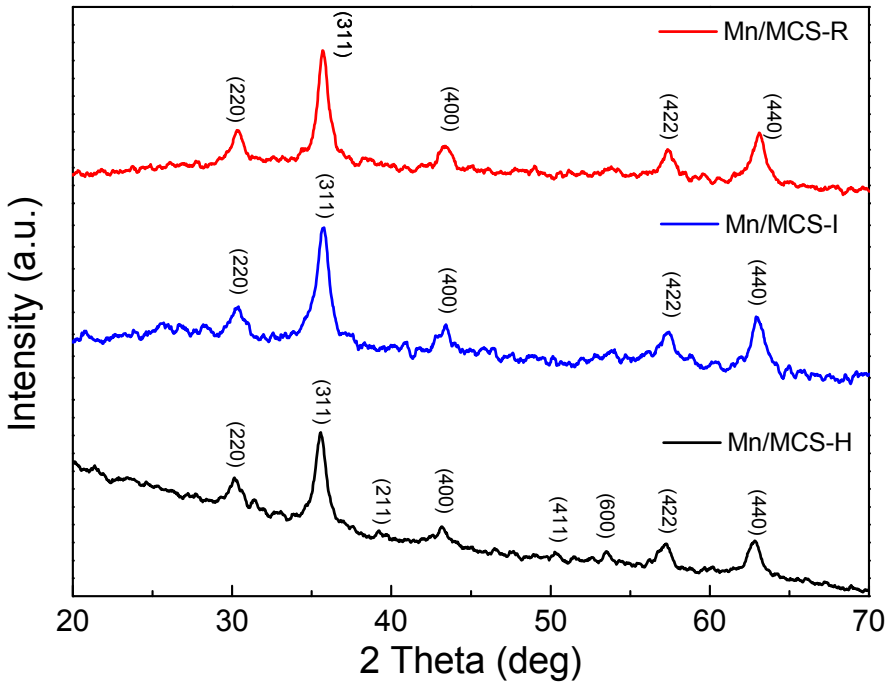

Figure 3. X-ray diffraction (XRD) patterns of various Fe_3O_4/C/Mn hybrids.

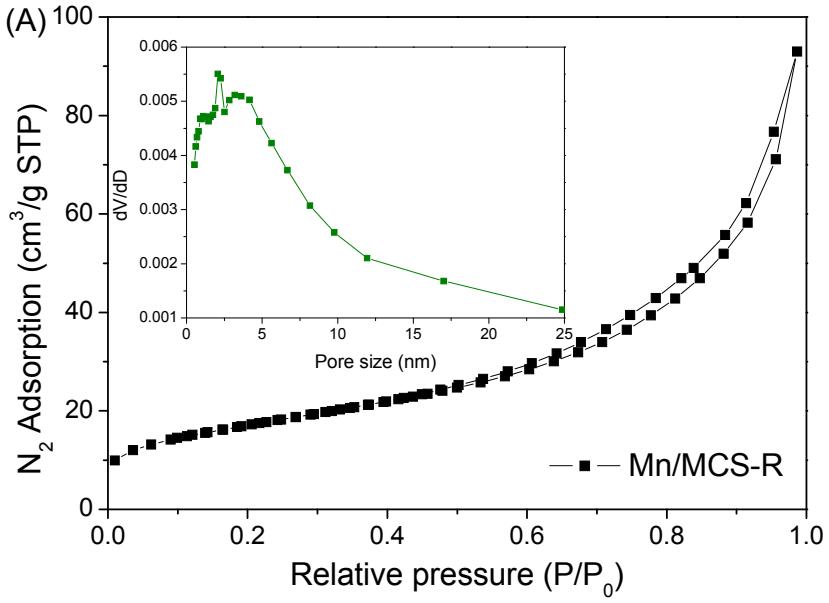

Figure 4. *Cont.*

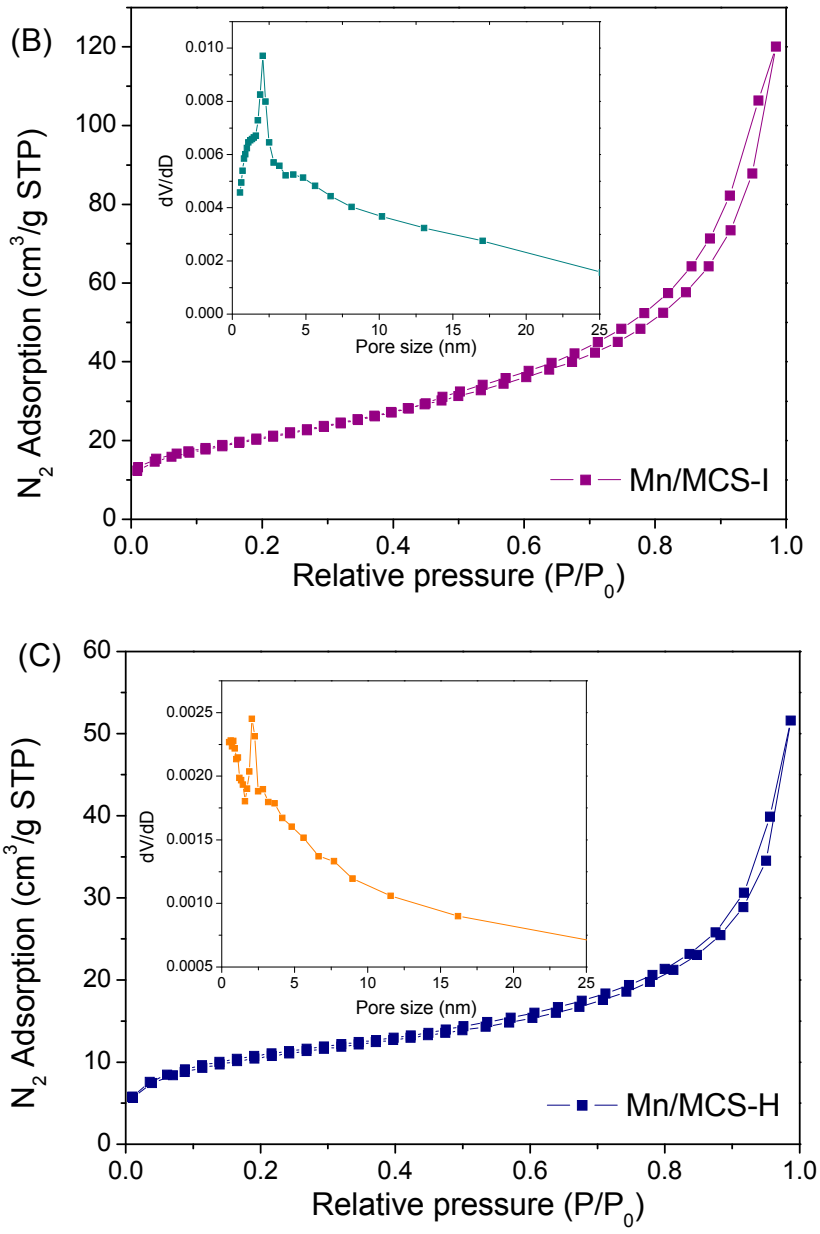

Figure 4. Nitrogen sorption isotherms and pore size distributions for Mn/MCS-R (**A**); Mn/MCS-I (**B**); Mn/MCS-H (**C**).

Table 1. Physicochemical properties of Fe_3O_4/C/Mn hybrids and their activities in phenol degradation.

Catalyst	Surface Area (S_{BET} m^2/g)	Pore Volume (cm^3/g)	First-Order Rate Constant (min^{-1})	R^2
Mn/MCS-R	53.8	0.11	0.074	0.996
Mn/MCS-I	74.6	0.14	0.052	0.989
Mn/MCS-H	26.6	0.058	0.056	0.991

FT-IR was employed to investigate the surface functional groups of the magnetic carbon sphere supported manganese catalysts (Figure 5). As seen, a broad band between 3600 and 3000 cm^{-1} was observed for all of the samples, which were resulted from the stretching vibration of the hydroxyl groups [28]. Besides hydroxyl groups, the intense peaks observed at 1699 and 1381 cm^{-1} in the spectra were attributed to the C=O and C–C vibrations, respectively [29]. The occurrence of these C=O and

C–C indicates the carbonization of glucose [30]. In addition, the IR band found at 579 cm^{-1} was assigned to the characteristic peaks of Fe–O vibration of Fe_3O_4 [31], which confirms the formation of magnetic core. However, compared with Mn/MCS-H, a new peak was created at 2150 cm^{-1} for the FT-IR spectra of annealed Mn/MCS samples (Mn/MCS-R and Mn/MCS-I), which is assigned to the creation of C≡C on the carbon surface during annealing process [32]. Moreover, compared with Mn/MCS-R and Mn/MCS-H, peak intensity of C–C vibration at 1381 cm^{-1} increase significantly for Mn/MCS-I, suggesting surface feature of MCS was reconstructed and more carbon atoms were connected by sp^3 hybridization after heat treatment.

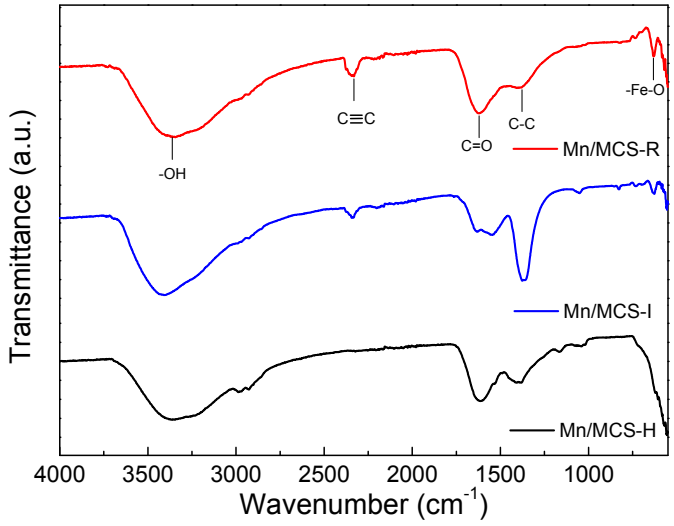

Figure 5. Fourier transform infrared spectroscopy (FT-IR) spectra of three Fe_3O_4/C/Mn hybrids.

Thermal stability of the three Fe_3O_4/C/Mn catalysts was investigated by TG-DTA under air flow (Figure 6). For TGA profiles of Mn/MCS-R and Mn/MCS-H (Figure 6A,C), three obvious weight processes were observed. A slight weight loss between 30 and 110 °C can be assigned to the removal of physically adsorbed water molecules. Further elevation of temperature caused a characteristic step/peak in the range from 250 to 400 °C which also reflects in a sharp peak on the heat flow, indicating the decomposition of carbon skeleton for the carbon coated on the Fe_3O_4 [33]. When temperature reached 500 °C, another slight weight loss was induced, indicating the oxidation of magnetic Fe_3O_4 core to Fe_2O_3. However, as seen in TGA profiles for Mn/MCS-I (Figure 6B), a three-stage weight loss process was observed. The first weight loss occurred before 300 °C, which could be attributed to the desorption of the surface adsorbed water. The second weight loss occurred between 400 and 600 °C, which is attributed to loss of lattice oxygen and the transforming of the oxidizing states. The final weight loss occurred between 750 and 850 °C, which could be ascribed to the further loss of the lattice oxygen and reduction to the Mn_3O_4, the most stable state of manganese oxide. The TGA pattern of Mn/MCS-I was quite similar as our previously reported α-MnO_2 [14]. Therefore, we presumed that the crystal form of Mn in Mn/MCS-I was α-MnO_2. In addition, the total weight loss was much less than those of Mn/MCS-R and Mn/MCS-H, suggesting that some of the carbon had been consumed during annealing in muffle furnace within sample synthesis processes. From the TG-DTA analysis, it can be deduced that manganese oxide in different oxidizing states has been formed for each of Fe_3O_4/C/Mn hybrid synthesized via different methods. Figure 6D shows the TGA curve of the fresh MCS. According to mass losses in the three Fe_3O_4/C/Mn hybrids, it could be calculated that the mass fractions of manganese oxide included in Mn/MCS-R, Mn/MCS-I and Mn/MCS-H was about 7.3%, 5.7% and 5.4%, respectively.

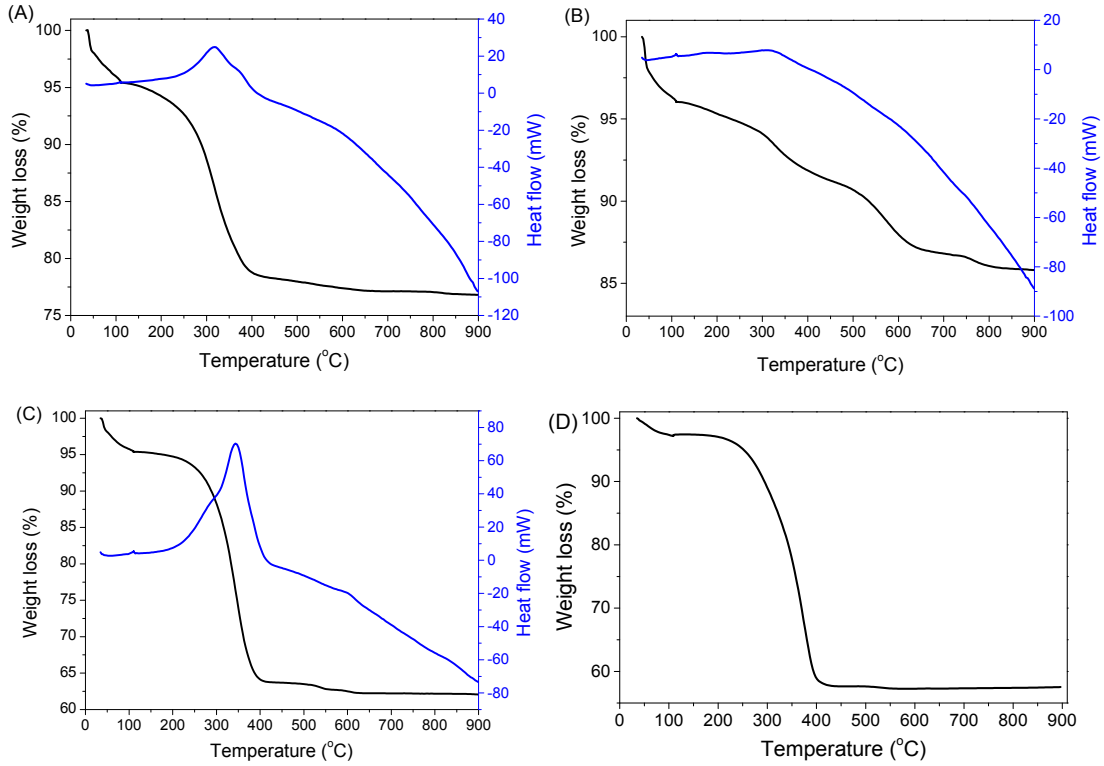

Figure 6. Thermogravimetric analysis (TGA) curves of Fe_3O_4/C/Mn hybrid: (**A**) Mn/MCS-R; (**B**) Mn/MCS-I; and (**C**) Mn/MCS-H (**D**) TGA curve of MCS.

2.2. Catalytic Oxidation of Phenol

Figure 7A describes the adsorption and phenol degradation on the three Fe_3O_4/C/Mn hybrids. In order to investigate the catalytic activity of the samples, control experiments were carried out to evaluate phenol removal caused by catalyst adsorption and PMS self-activation at ambient environment. Without any catalyst, PMS induced negligible phenol degradation by itself. Shown in the figure, less than 10% of phenol was removed after 180 min, revealing that PMS itself could not be effectively activated by the ambient environment to produce reactive species for significant phenol degradation. For the adsorption tests carried out with the presence of catalysts only, three catalysts showed similar phenol removal profiles, in which phenol removal fluctuated for the first 60 min to achieve adsorption/desorption equilibrium. However, subsequently these catalysts did not show any significant phenol degradation. For phenol removal profiles of catalytic reactions, commercial MnO_2 presented phenol removal at 20%. Mn/MCS-R with PMS provided the best phenol degradation rate and 100% removal of phenol was achieved within 180 min. While phenol degradation for both Mn/MCS-I and Mn/MCS-H with PMS were similar and around 90% of the initial phenol was removed after 180 min.

Control experiments were carried out to investigate the catalytic activities of the carbon sphere, Fe_3O_4, MCS and MnO_x (Figure 7B). As seen, carbon sphere demonstrated significant capability for phenol adsorption due to its highly porous structure. However, its catalytic degradation profile almost overlapped the adsorption profile, indicating the negligible catalytic activity. Fe_3O_4 displayed insignificant phenol adsorption capability and catalytic activity since less than 10% of phenol was removed after 180 min for both conditions. MCS showed some catalytic activity, however, still incomparable with those of Mn/MCSs'. MnO_x was obtained by calcination of $MnSO_4 \cdot H_2O$ at 200 °C for 4 h. As observed, around 85% of the phenol was decomposed when MnO_x was utilized as the catalyst for PMS activation.

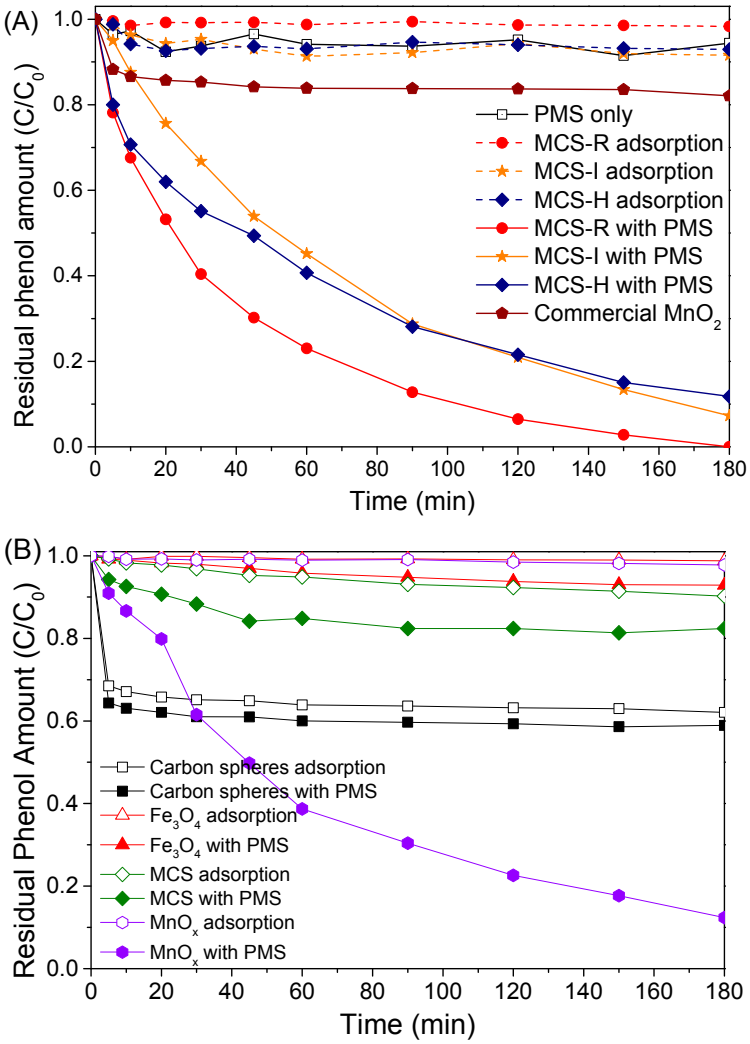

Figure 7. Residual phenol amount using MCS related catalysts (**A**) and other control factors (**B**) (C/C_0) as revealed by high performance liquid chromatography (HPLC) (270 nm wavelength). Reaction condition: $[\text{phenol}]_0$ = 20 mg/L, catalyst loading = 0.2 g/L, Oxone loading = 2.0 g/L, Temperature: 25 °C.

Based on these phenol degradation profiles, a first order kinetic mode (Equation (1)) was applied to evaluate the catalytic reaction kinetics.

$$ln\left(\frac{C}{C_0}\right) = -kt \quad (1)$$

where C is phenol concentration at time (t) and C_0 is the phenol concentration at initial time. K is the first order reaction rate constant. Figure 8 shows that phenol degradation curve was well fitted ($R^2 > 0.98$) with the first-order kinetics.

The catalytic activities of these as-synthesized supported manganese catalysts does not seem to be correlated with their surface areas. In fact, the highest BET specific surface area of Mn/MCS-I (74.6 m^2/g) did not lead to the fastest reaction rate, as well as this materials showed a similar catalytic activity as that of Mn/MCS-H, although its BET surface area was around 3 times less than Mn/MCS-I (26 m^2/g vs. 75 m^2/g). Remarkably, Mn/MCS-R, which had a surface area of 53.8 m^2/g, displayed the highest catalytic activity and the reaction rate constant.

Several studies also revealed that the catalytic activities of supported metal oxides were independent on the surface area [34,35]. Cobalt oxides loaded on Al_2O_3, SiO_2 and TiO_2 were prepared by Sun et al. and their activities were tested for phenol degradation [34]. It was found that, even though Co/TiO_2 possessed the least surface area, it demonstrated the highest catalytic activity for decomposition of phenol. Wang et al. synthesized $MnO_2/ZnFe_2O_4$ magnetic catalysts with different shapes for environmental remediation purposes [36]. Compared with the sea-urchin shaped catalyst, the corolla shaped catalysts showed lower BET specific surface area but superior catalytic activities for activation of PMS for phenol degradation. In this study, TGA results suggested that the order of catalytic activity on these catalysts are well in agreement with their corresponding manganese oxide loading amount. Mn/MCS-R, obtaining the greatest manganese oxide loading amount (7.3%), showed the highest catalytic activity.

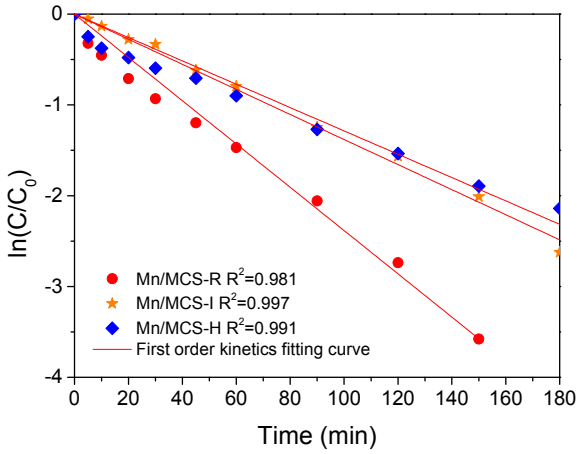

Figure 8. First order kinetic model of reactions. *Y* axis values are referred to the residual phenol.

In the past few years, investigations have been carried out for both homogeneous and heterogeneous catalytic reactions using Mn based catalysts. Anipsitakis and Dionysiou [37] used Mn^{2+} for homogeneous activation of PMS for 2,4-dichlorophenol (2,4-DCP) degradation. In their studies, 24% of initial amount of 2,4-DCP was removed within 4 h when HSO_5^- concentration was 50 ppm. Watts et al. [6] investigated oxidative and reductive pathways in manganese-catalyzed Fenton reactions and found that reducing species were generated by crystalline and amorphous MnO_2-catalysed decomposition of H_2O_2. Edy et al. [38] synthesized α-Mn_2O_3 in different shapes using a one-step hydrothermal method and investigated their catalytic activities for activation of PMS to degrade phenol. They found that α-Mn_2O_3 cubic possessed the best catalytic activity and for 25 ppm phenol, 100% decomposition achieved within 60 min when catalyst usage of 0.4 g/L. Liang et al. [15] reported mesoporous MnO_2 supported Co_3O_4 nanoparticles synthesized by impregnation and their performances in heterogeneous activation of peroxymonosulfate (PMS) for phenol degradation. They found that when Co_3O_4 loading rate is 3 wt %, MnO_2 supported Co_3O_4 catalysts could achieve 100% phenol removal at phenol concentration of 25 ppm within 120 min.

It has been proposed that PMS activation process was induced by redox reactions [14], while the transition of Mn^{4+}/Mn^{3+} provides the redox potential. Thus, the mechanism of catalytic oxidation of phenol on $Fe_3O_4/C/Mn$ hybrids with PMS could be proposed as follows.

$$S-Mn(IV) + HSO_5^- \rightarrow S-Mn(III) + SO_4^- + OH^- \ (S-solid) \quad (2)$$

$$S-Mn(III) + HSO_5^- \rightarrow S-Mn(IV) + SO_5^- + H^+ \ (S-solid) \quad (3)$$

$$SO_4^- + H_2O \rightarrow SO_4^{2-} + OH\cdot + H^+ \quad (4)$$

$$SO_4^- + OH\cdot + C_6H_5OH \rightarrow \text{serveral steps} \rightarrow CO_2 + H_2O + SO_4^{2-} \quad (5)$$

Figure 9 shows photographs of Fe_3O_4/C/Mn catalysts when they were dispersed in water and were separated by an external magnetic field. As seen, all of the catalysts could be well dispersed to form stable brown suspension after a 1 min long sonication (Figure 9A). When a magnet was approached, catalysts in each of the glass vials accumulated to the side near the magnet quickly. The solution became clear within 2 min (Figure 9B). After the magnetic was removed and as-mentioned sonicating procedure was repeated, all three samples re-dispersed in water and formed the stable suspension again. Therefore, since attraction and dispersion processes can be readily altered by simply approaching or removing an external magnetic field, the as-synthesized Fe_3O_4/C/Mn catalysts demonstrated excellent water dispersion and magnetic separation ability for effective separation.

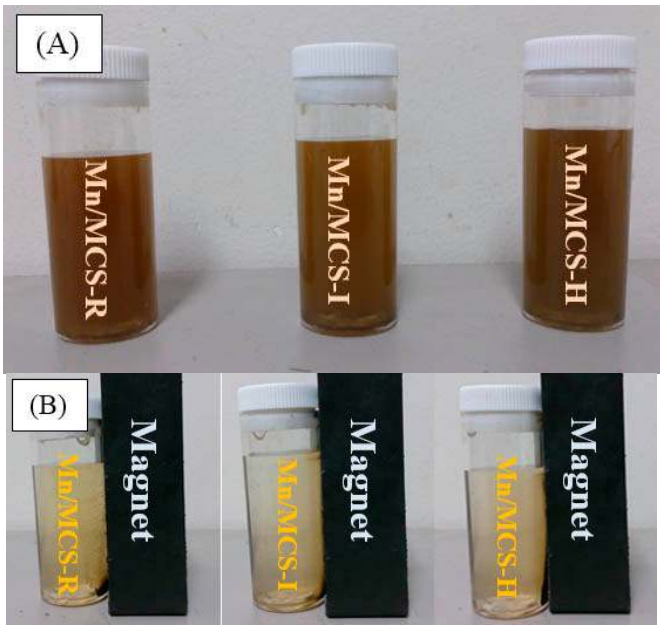

Figure 9. Photographs of the separation and dispersion processes: (**A**) without external magnetic field; and (**B**) with external magnetic field.

In order to evaluate the influence of reaction conditions on catalytic phenol degradation, further studies were carried out using the most effective catalyst, Mn/MCS-R. Figure 10 illustrates phenol degradation on Mn/MCS-R as a function of different temperatures (25, 35, and 45 °C). As shown in the figure, phenol degradation rate was enhanced when reaction temperature was elevated, indicating the endothermic property of this catalytic reaction. Higher temperature induced the production of more reactive species. The time intervals necessary to guarantee 100% phenol degradation were 120 and 60 min at the temperatures of 35 and 45 °C, respectively. Based on the first-order kinetics, reaction rate constants at varying temperatures were obtained and they were related with temperature by the Arrhenius equation with high regression coefficients, shown in the inset figure. The activation energy was then calculated to be 32.1 kJ/mol.

Previously, very few investigations have been reported on supported MnO*x* catalysts on activation of PMS for phenol degradation. However, in recent years, investigations were carried out for heterogeneous activation of PMS using supported cobalt oxide as catalysts. Very recently, we investigated the catalytic activity of magnetic cobalt/carbon sphere/Fe_3O_4 composites (Co/MCS) for catalytic oxidation of phenol, and found the activation energy at 49.1 kJ/mol [24]. For comparison, Table 2 summarizes the activation energies obtained from these researches on PMS activation using supported cobalt oxide as catalysts. As seen, activation energies of supported cobalt oxide catalysts are within the range of 40–70 kJ/mol and thus the as-synthesized supported manganese oxide catalyst (Mn/MCS-R) presents much lower activation energy.

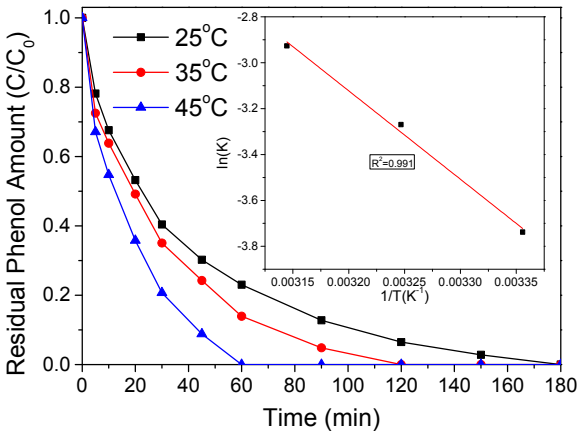

Figure 10. Phenol degradation on Mn/MCS-R at different reaction temperature. Reaction conditions: $[phenol]_0$ = 20 mg/L, catalyst loading = 0.2 g/L, Oxone loading = 2.0 g/L.

Table 2. Activation energies of representative Mn- and Co-based catalysts.

Catalyst	Activation Energy (kJ/mol)	Reference
Co/MCS	49.1	[24]
Co/carbon xerogel	48.3	[39]
Co/MnO_2	42.5	[15]
Co/activated carbon	59.7	[40]
Co/red mud	47.2	[41]
Co/SBA-15	67.4	[42]
Fe_3O_4/C/Mn hybrids	32.1	This study

Figure 11 presents the catalytic activity of regenerated Mn/MCS-R by simple water washing in phenol degradation. In the second run, the significant decrease in catalytic activity was observed and 80% of initial phenol was degraded after 180 min, which indicates the deactivation of the catalyst. For the third run, catalytic activity further decreased and around 40% of initial phenol remained after the reaction. The decrease of catalytic activity can be assigned to the attachment of reaction intermediates on the catalyst surface with active sites. Moreover, due to the strong van de Waals force, these intermediates cannot be fully removed by simple water washing. In addition, the passivation of the catalyst might be resulted from the composition change of the Mn valence states.

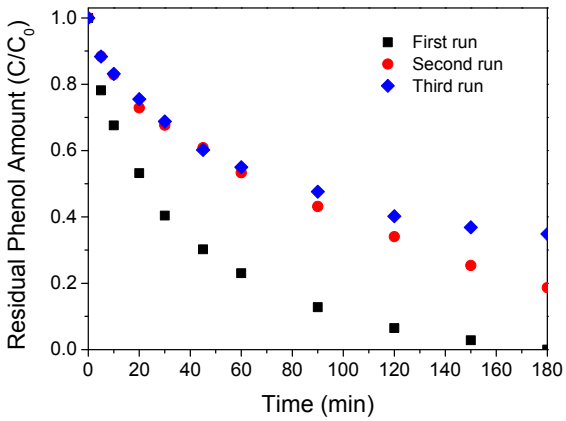

Figure 11. Phenol degradation on Mn/MCS-R at different runs after recycling. Reaction conditions: $[phenol]_0$ = 20 mg/L, catalyst loading = 0.2 g/L, Oxone loading = 2.0 g/L, and T = 25 °C.

To better evaluate the versatility of the as-prepared materials, catalytic degradation tests employing *p*-cresol and *p*-nitrophenol as the target pollutants were carried out (Figure 12) For *p*-cresol and *p*-nitrophenol, since the *para*-position of the phenol was substituted by a methyl group and a nitro group, respectively, the influence of electron donating group (EDG)-methyl group, and electron withdrawing group (EWG)-nitro group, on the degradation efficiency was evaluated. As seen, both *p*-cresol and *p*-nitrophenol demonstrated the inertness for PMS attacking, which was similar as the phenol. This recalcitrance suggested that with the involvement of EDG or EWG, PMS is not favorable for neither electrophilic attack nor nucleophilic attack on the aromatic ring. However, with the presence of catalysts, the degradation efficiency for the target pollutants differed. Compared with phenol, *p*-nitrophenol displayed some recalcitrance for catalytic PMS degradation and around 15% of which was still remained in the reaction solution at the end of 180 min. *P*-cresol demonstrated a higher reaction rate than phenol and complete degradation occurred at 90 min. As discussed, sulfate and hydroxyl radicals, which are electrophilic, were the main active species generated from PMS activation. The involvement of methyl group (EWG) on the aromatic ring could be beneficial for attracting these electrophilic reactive species since the electrons from the methyl group improved the nucleophilicity of the aromatic ring. In contrast, the substituted EWG groups on the aromatic ring hindered this nucleophilicity of the aromatic ring and creating the resistance for the attacking from sulfate and hydroxyl radicals.

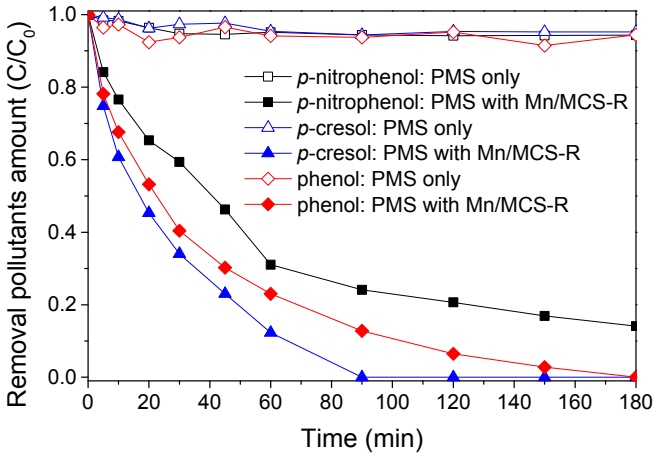

Figure 12. Effects of electron withdrawing group (EWG) and electron donating group (EDG) on degradation efficiency. Reaction conditions: $[p\text{-nitrophenol}]_0$ = 20 mg/L, $[\text{phenol}]_0$ = 50 ppm, $[p\text{-cresol}]_0$ = 20 ppm, $[p\text{-chlorophenol}]_0$ = 50 ppm, catalyst loading = 0.2 g/L, PMS loading: 2 g/L, temperature: 25 °C.

3. Materials and Methods

3.1. Materials

Iron (II) chloride tetrahydrate (99.9%), iron (III) hexahydrate (99.9%), manganese sulfate monohydrate (99.8%) and potassium permanganate (99.8%) were purchased from Sigma Aldrich. D-glucose (99.9%) was obtained from Fluka. Ammonia solution (28%) was obtained from Ajax Finechem. High purity nitrogen gas (99%) was obtained from BOC (WA, Australia). All chemicals were used as received without any further purification.

3.2. Synthesis of Manganese Loaded Magnetic Carbon Spheres (Fe_3O_4/C/Mn)

Magnetic carbon nanospheres were synthesized via a modified hydrothermal method, and detailed procedures can be found in our recent publication [24]. The obtained sample was labeled as MCS. In a typical synthesis of redox method, 1.5 g of MCS were put into a quartz boat and then

transferred to a muffle furnace for annealing in air at 200 °C for 1 h. Then, 0.5 g annealed MCS was mixed with 0.11 g (0.07 mol) $KMnO_4$ in a beaker. The mixture was dispersed in 50 mL of ultrapure water under sonication for 10 min. Then the beaker was immerged in a water bath at 70 °C and kept stirring for 4 h. The resulting brownish precipitate was filtered and washed with ultrapure water for three times and dried in an oven at 80 °C overnight. The sample was marked as Mn/MCS-R.

In the synthesis of impregnation method, 0.5 g MCS was dispersed in 50 mL of ethanol under sonication for 10 min. Then, 0.12 g (0.07 mol) $MnSO_4 \cdot H_2O$ was added in the as-dispersed MCS solution. The mixed solution was stirred overnight to ensure the fully evaporation of ethanol. The resulted mixture solid was then transferred to a muffle furnace to anneal in air at 200 °C for 4 h. After that the annealed mixture was washed with ultrapure water for three times and dried in an oven at 80 °C overnight. The sample was denoted as Mn/MCS-I.

For hydrothermal method, 0.5 g MCS was dispersed in 80 mL of ultrapure water under sonication for 10 min. Then, 0.12 g (0.07 mol) $MnSO_4 \cdot H_2O$ was added in the as-dispersed MCS solution. The mixed solution was stirred for at least 30 min to ensure the homogeneous dispersion. Then the mixed solution was transferred into a Teflon-lined stainless steel autoclave with the capacity of 120 mL. The autoclave was then sealed and maintained at 140 °C for 12 h and was then cooled down to room temperature naturally. The products were harvested by vacuum filtration and washed with ultrapure water for 3 times before being dried at 80 °C overnight. The obtained samples were denoted as Mn/MCS-H.

To compare, carbon microspheres, Fe_3O_4 and MnO_x were synthesized. Carbon microspheres were synthesized by hydrothermal pyrolysis of glucose at 180 °C for 18 h. For preparation of Fe_3O_4 nanoparticles, $FeCl_3$ and $FeCl_2$ at the molar ratio of 2:1 were dissolved in the ultrapure water. After the mixture solution was bubbled with nitrogen flow for 10 min, 28% ammonia solution was added dropwisely to make solution pH 10. After stirring for 1 h, Fe_3O_4 nanoparticles were harvested by filtering the mixture solution and washed by ultrapure water/ethanol for 3 times. Manganese oxide was obtained by calcination of $MnSO_4 \cdot H_2O$ at 200 °C for 4 h and labeled ad MnO_x.

3.3. Characterization of Materials

The morphology and chemical compositions of the catalysts were observed on a ZEISS NEON 40EsB Field Emission Scanning Electron Microscope (FESEM, ZEISS, Germany). XRD patterns were obtained on a Bruker D8 (Bruker-AXS, Karlsruhe, Germany) diffractometer using a filtered CuKa radiation (λ = 1.5418 Å) with an accelerating voltage of 40 kV and current of 30 mA. N_2 adsorption/desorption was measured using a Micromeritics Tristar 3000 (Micromeritics, GA USA) to obtain pore volume and the Brunauer-Emmett-Teller (BET) specific surface area. Prior to measurement, the samples were degassed at 120 °C for 5 h under vacuum condition. Fourier transform infrared (FT-IR) spectra were obtained from a Perkin-Elmer Spectroscopy (Perkin-Elmer, UK) 100 with a resolution of 4 cm^{-1} in transmission mode at room temperature. The Mn content and thermal stability of Mn/MCS and reference materials were investigated using thermal gravimetric analysis-differential scanning calorimetry (TGA-DSC, Mettler-Toledo, Switzerland) in air on a Mettler-Toledo Star^e system. The air flow rate was 100 mL/min and the heating rate was 10 °C/min.

3.4. Catalytic Activity Tests

The catalytic oxidation of phenol was carried out in a 500 mL reactor containing 20 ppm of phenol solution with a constant stirring of 400 rpm. The reactor was attached to a stand and dipped in a water bath with a temperature controller. Unless specifically stated, the reaction temperature was 25 °C. In a typical test, firstly, 0.1 g catalyst was added into the phenol solution and stirred for 30 min to achieve adsorption-desorption equilibrium, then Oxone® ($2KHSO_5 \cdot KHSO_4 \cdot K_2SO_4$, PMS, obtained from Aldrich) was added into the solution at 2 g/L. At certain time, 1 mL sample was withdrawn by a syringe and filtered into a HPLC vial, which was added of 0.5 mL methanol to quench the reaction. The concentration of phenol was analyzed by a Varian HPLC with a UV detector and a wavelength set

at 270 nm. A C-18 column was used to separate the organics while the mobile phase with a flow rate of 1 mL/min was made of 30% CH_3CN and 70% water.

4. Conclusions

Fe_3O_4/C/Mn catalysts were synthesized using redox, impregnation and hydrothermal methods, respectively. The catalytic activities of these magnetically separable Mn based catalysts (Mn/MCS) were tested for activation of PMS in producing oxidative radicals for degradation of phenol. It was found that Fe_3O_4/C/Mn hybrids synthesized by redox method showed the best catalytic activity. Moreover, all of the as-prepared Mn catalysts presented a higher activity than commercial MnO_2 catalysts. Phenol catalytic degradation on these supported Mn catalysts followed the first order reaction kinetics and the activation energy of phenol degradation on Fe_3O_4/C/Mn hybrids synthesized by the redox method was 32.1 kJ/mol. This study provided a feasible approach for removal of organic pollutants by magnetically separable catalysts.

Acknowledgments: The authors greatly appreciate the financial supports from the National Natural Science Youth Foundation of China (No. 21606253) and Science Foundation of China University of Petroleum, Beijing (No. 2462016YJRC013). The authors also acknowledge the use of equipment as well as scientific and technical assistance of the Curtin University Electron Microscope Facility and Centre for Microscopy Characterization, which have been partially funded by the University, State and Commonwealth Governments.

Author Contributions: Y.W. and H.S. conceived and designed the experiments; Y.W. and X.D. performed the experiments; Y.W. and C.C. analyzed the data; S.W. and Y.X. contributed reagents/materials/analysis tools; Y.W. wrote the paper.

Conflicts of Interest: The authors declare no conflict of interest.

References

1. Gupta, V.K.; Ali, I.; Saleh, T.A.; Nayak, A.; Agarwal, S. Chemical treatment technologies for waste-water recycling—An overview. *RSC Adv.* **2012**, *2*, 6380–6388. [CrossRef]
2. Gupta, V.K.; Srivastava, S.K.; Tyagi, R. Design parameters for the treatment of phenolic wastes by carbon columns (obtained from fertilizer waste material). *Water Res.* **2000**, *34*, 1543–1550. [CrossRef]
3. Heng, S.; Yeung, K.L.; Julbe, A.; Ayral, A.; Schrotter, J.-C. Preparation of composite zeolite membrane separator/contactor for ozone water treatment. *Microporous Mesoporous Mater.* **2008**, *115*, 137–146. [CrossRef]
4. Tušar, N.N.; Maučec, D.; Rangus, M.; Arčon, I.; Mazaj, M.; Cotman, M.; Pintar, A.; Kaučič, V. Manganese functionalized silicate nanoparticles as a fenton-type catalyst for water purification by advanced oxidation processes (AOP). *Adv. Funct. Mater.* **2012**, *22*, 820–826. [CrossRef]
5. Wang, S. A comparative study of fenton and fenton-like reaction kinetics in decolourisation of wastewater. *Dyes Pigm.* **2008**, *76*, 714–720. [CrossRef]
6. Watts, R.; Sarasa, J.; Loge, F.; Teel, A. Oxidative and reductive pathways in manganese-catalyzed fenton's reactions. *J. Environ. Eng.* **2005**, *131*, 158–164. [CrossRef]
7. Hu, L.; Yang, X.; Dang, S. An easily recyclable Co/SBA-15 catalyst: Heterogeneous activation of peroxymonosulfate for the degradation of phenol in water. *Appl. Catal. B* **2011**, *102*, 19–26. [CrossRef]
8. Anipsitakis, G.P.; Dionysiou, D.D. Degradation of organic contaminants in water with sulfate radicals generated by the conjunction of peroxymonosulfate with cobalt. *Environ. Sci. Technol.* **2003**, *37*, 4790–4797. [CrossRef] [PubMed]
9. Rastogi, A.; Al-Abed, S.R.; Dionysiou, D.D. Sulfate radical-based ferrous-peroxymonosulfate oxidative system for PCBs degradation in aqueous and sediment systems. *Appl. Catal. B* **2009**, *85*, 171–179. [CrossRef]
10. Anipsitakis, G.P.; Dionysiou, D.D.; Gonzalez, M.A. Cobalt-mediated activation of peroxymonosulfate and sulfate radical attack on phenolic compounds. Implications of chloride ions. *Environ. Sci. Technol.* **2005**, *40*, 1000–1007. [CrossRef]
11. Tsitonaki, A.; Petri, B.; Crimi, M.; MosbÆK, H.; Siegrist, R.L.; Bjerg, P.L. In situ chemical oxidation of contaminated soil and groundwater using persulfate: A review. *Crit. Rev. Env. Sci. Technol.* **2010**, *40*, 55–91. [CrossRef]

12. Shukla, P.; Sun, H.; Wang, S.; Ang, H.M.; Tadé, M.O. Nanosized Co_3O_4/SiO_2 for heterogeneous oxidation of phenolic contaminants in waste water. *Sep. Purif. Technol.* **2011**, *77*, 230–236. [CrossRef]
13. Saputra, E.; Muhammad, S.; Sun, H.; Ang, H.-M.; Tadé, M.O.; Wang, S. A comparative study of spinel structured Mn_3O_4, Co_3O_4 and Fe_3O_4 nanoparticles in catalytic oxidation of phenolic contaminants in aqueous solutions. *J. Colloid Interface Sci.* **2013**, *407*, 467–473. [CrossRef] [PubMed]
14. Saputra, E.; Muhammad, S.; Sun, H.Q.; Ang, H.M.; Tadé, M.O.; Wang, S.B. Different crystallographic one-dimensional MnO_2 nanomaterials and their superior performance in catalytic phenol degradation. *Environ. Sci. Technol.* **2013**, *47*, 5882–5887. [CrossRef] [PubMed]
15. Sun, H.; Liu, S.; Zhou, G.; Ang, H.M.; Tadé, M.O.; Wang, S. Reduced graphene oxide for catalytic oxidation of aqueous organic pollutants. *ACS Appl. Mater. Interfaces* **2012**, *4*, 5466–5471. [CrossRef] [PubMed]
16. Yao, Y.; Yang, Z.; Sun, H.; Wang, S. Hydrothermal synthesis of Co_3O_4-graphene for heterogeneous activation of peroxymonosulfate for decomposition of phenol. *Ind. Eng. Chem. Res.* **2012**, *51*, 14958–14965. [CrossRef]
17. Gong, J.-L.; Wang, B.; Zeng, G.-M.; Yang, C.-P.; Niu, C.-G.; Niu, Q.-Y.; Zhou, W.-J.; Liang, Y. Removal of cationic dyes from aqueous solution using magnetic multi-wall carbon nanotube nanocomposite as adsorbent. *J. Hazard. Mater.* **2009**, *164*, 1517–1522. [CrossRef] [PubMed]
18. Zhang, P.; Zhan, Y.; Cai, B.; Hao, C.; Wang, J.; Liu, C.; Meng, Z.; Yin, Z.; Chen, Q. Shape-controlled synthesis of Mn_3O_4 nanocrystals and their catalysis of the degradation of methylene blue. *Nano Res.* **2010**, *3*, 235–243. [CrossRef]
19. Kaminski, M.D.; Nuñez, L. Extractant-coated magnetic particles for cobalt and nickel recovery from acidic solution. *J. Magn. Magn. Mater.* **1999**, *194*, 31–36. [CrossRef]
20. Chen, C.; Hu, J.; Shao, D.; Li, J.; Wang, X. Adsorption behavior of multiwall carbon nanotube/iron oxide magnetic composites for Ni(II) and Sr(II). *J. Hazard. Mater.* **2009**, *164*, 923–928. [CrossRef] [PubMed]
21. Yao, Y.J.; Miao, S.D.; Liu, S.Z.; Ma, L.P.; Sun, H.Q.; Wang, S.B. Synthesis, characterization, and adsorption properties of magnetic Fe_3O_4@graphene nanocomposite. *Chem. Eng. J.* **2012**, *184*, 326–332. [CrossRef]
22. Lu, Z.; Dai, J.; Song, X.; Wang, G.; Yang, W. Facile synthesis of Fe_3O_4/SiO_2 composite nanoparticles from primary silica particles. *Colloids Interface A* **2008**, *317*, 450–456. [CrossRef]
23. Cheng, Y.; Tan, R.; Wang, W.; Guo, Y.; Cui, P.; Song, W. Controllable synthesis and magnetic properties of Fe_3O_4 and Fe_3O_4@SiO_2 microspheres. *J. Mater. Sci* **2010**, *45*, 5347–5352. [CrossRef]
24. Wang, Y.; Sun, H.; Ang, H.M.; Tadé, M.O.; Wang, S. Magnetic Fe_3O_4/carbon sphere/cobalt composites for catalytic oxidation of phenol solutions with sulfate radicals. *Chem. Eng. J.* **2014**, *245*, 1–9. [CrossRef]
25. Wang, Y.; Sun, H.; Ang, H.M.; Tadé, M.O.; Wang, S. Synthesis of magnetic core/shell carbon nanosphere supported manganese catalysts for oxidation of organics in water by peroxymonosulfate. *J. Colloid Interface Sci.* **2014**, *433*, 68–75. [CrossRef] [PubMed]
26. Dey, R.; Mukherjee, N.; Ahammed, S.; Ranu, B.C. Highly selective reduction of nitroarenes by iron(0) nanoparticles in water. *Chem. Commun.* **2012**, *48*, 7982–7984. [CrossRef] [PubMed]
27. Xiao, W.; Wang, D.; Lou, X.W. Shape-controlled synthesis of MnO_2 nanostructures with enhanced electrocatalytic activity for oxygen reduction. *J. Phys. Chem. C* **2009**, *114*, 1694–1700. [CrossRef]
28. Xu, J.; Chu, W.; Luo, S. Synthesis and characterization of mesoporous V-MCM-41 molecular sieves with good hydrothermal and thermal stability. *J. Mol. Catal. A: Chem.* **2006**, *256*, 48–56. [CrossRef]
29. Titirici, M.M.; Thomas, A.; Antonietti, M. Replication and coating of silica templates by hydrothermal carbonization. *Adv. Funct. Mater.* **2007**, *17*, 1010–1018. [CrossRef]
30. Sevilla, M.; Fuertes, A.B. The production of carbon materials by hydrothermal carbonization of cellulose. *Carbon* **2009**, *47*, 2281–2289. [CrossRef]
31. Ai, Z.; Deng, K.; Wan, Q.; Zhang, L.; Lee, S. Facile microwave-assisted synthesis and magnetic and gas sensing properties of Fe_3O_4 nanoroses. *J. Phys. Chem. C* **2010**, *114*, 6237–6242. [CrossRef]
32. Huang, Y.; Dong, Z.; Jia, D.; Guo, Z.; Cho, W.I. Preparation and characterization of core-shell structure Fe_3O_4/C nanoparticles with unique stability and high electrochemical performance for lithium-ion battery anode material. *Electrochim. Acta* **2011**, *56*, 9233–9239. [CrossRef]
33. Wang, J.; Zheng, S.; Shao, Y.; Liu, J.; Xu, Z.; Zhu, D. Amino-functionalized Fe_3O_4@SiO_2 core-shell magnetic nanomaterial as a novel adsorbent for aqueous heavy metals removal. *J. Colloid Interface Sci.* **2010**, *349*, 293–299. [CrossRef] [PubMed]
34. Sun, H.; Liang, H.; Zhou, G.; Wang, S. Supported cobalt catalysts by one-pot aqueous combustion synthesis for catalytic phenol degradation. *J. Colloid Interface Sci.* **2013**, *394*, 394–400. [CrossRef] [PubMed]

35. Huang, Z.; Bao, H.; Yao, Y.; Lu, W.; Chen, W. Novel green activation processes and mechanism of peroxymonosulfate based on supported cobalt phthalocyanine catalyst. *Appl. Catal. B* **2014**, *154–155*, 36–43. [CrossRef]
36. Wang, Y.; Sun, H.; Ang, H.M.; Tadé, M.O.; Wang, S. Facile synthesis of hierarchically structured magnetic MnO_2/$ZnFe_2O_4$ hybrid materials and their performance in heterogeneous activation of peroxymonosulfate. *ACS Appl. Mater. Interfaces* **2014**, *6*, 19914–19923. [CrossRef] [PubMed]
37. Anipsitakis, G.P.; Dionysiou, D.D. Radical generation by the interaction of transition metals with common oxidants. *Environ. Sci. Technol.* **2004**, *38*, 3705–3712. [CrossRef] [PubMed]
38. Saputra, E.; Muhammad, S.; Sun, H.; Ang, H.-M.; Tadé, M.O.; Wang, S. Shape-controlled activation of peroxymonosulfate by single crystal α-Mn_2O_3 for catalytic phenol degradation in aqueous solution. *Appl. Catal. B* **2014**, *154–155*, 246–251. [CrossRef]
39. Sun, H.; Tian, H.; Hardjono, Y.; Buckley, C.E.; Wang, S. Preparation of cobalt/carbon-xerogel for heterogeneous oxidation of phenol. *Catal. Today* **2012**, *186*, 63–68. [CrossRef]
40. Shukla, P.R.; Wang, S.; Sun, H.; Ang, H.M.; Tadé, M. Activated carbon supported cobalt catalysts for advanced oxidation of organic contaminants in aqueous solution. *Appl. Catal. B* **2010**, *100*, 529–534. [CrossRef]
41. Saputra, E.; Muhammad, S.; Sun, H.; Ang, H.M.; Tadé, M.O.; Wang, S. Red mud and fly ash supported Co catalysts for phenol oxidation. *Catal. Today* **2012**, *190*, 68–72. [CrossRef]
42. Shukla, P.; Sun, H.; Wang, S.; Ang, H.M.; Tadé, M.O. Co-SBA-15 for heterogeneous oxidation of phenol with sulfate radical for wastewater treatment. *Catal. Today* **2011**, *175*, 380–385. [CrossRef]